



CHORUS

This is the accepted manuscript made available via CHORUS. The article has been published as:

Dynamics of signal propagation and collision in axons

Rosangela Follmann, Epaminondas Rosa, Jr., and Wolfgang Stein

Phys. Rev. E **92**, 032707 — Published 14 September 2015

DOI: [10.1103/PhysRevE.92.032707](https://doi.org/10.1103/PhysRevE.92.032707)

Dynamics of Signal Propagation and Collision in Axons

Rosangela Follmann,¹ Epaminondas Rosa, Jr.,² and Wolfgang Stein^{1,*}

¹*School of Biological Sciences, Illinois State University, Normal, IL 61790, USA*

²*Department of Physics, Illinois State University, Normal, IL 61790, USA*

(Dated: August 31, 2015)

Long-range communication in the nervous system is usually carried out with the propagation of action potentials along the axon of nerve cells. While typically thought of as being unidirectional, it is not uncommon for axonal propagation of action potentials to happen in both directions. This is the case because action potentials can be initiated at multiple ‘ectopic’ positions along the axon. Two ectopic action potentials generated at distinct sites, and traveling toward each other, will collide. As neuronal information is encoded in the frequency of action potentials, action potential collision and annihilation may affect the way in which neuronal information is received, processed and transmitted. We investigate action potential propagation and collision using an axonal multicompartment model based on the Hodgkin-Huxley equations. We characterize propagation speed, refractory period, excitability and action potential collision for slow (type I) and fast (type II) axons. In addition, our studies include experimental measurements of action potential propagation in axons of two biological systems. Both computational and experimental results unequivocally indicate that colliding action potentials do not pass each other, they are reciprocally annihilated.

PACS numbers: 87.19.lb

I. INTRODUCTION

Neurons are electrically excitable cells capable of receiving, processing and transmitting information. Long distance neuronal communication is achieved via action potentials which are fast occurrences of rise and fall of the voltage across the cell membrane. Action potentials are the result of complex electro-chemical mechanisms controlling the opening and closing of selective ion channels [1], and are usually generated at the axon hillock - a site located adjacent to the neuron’s cell body. Ectopic action potentials, initiated at a spike initiation zone located on the axon away from the hillock [2–6], are less known despite the fact that they are prevalent in many neural systems, including the cerebral cortex [7]. They travel in two opposite directions: *orthodromically*, toward the axon terminal, and *antidromically*, toward the cell body. Ectopic firing frequencies are typically lower than those generated at the hillock. When both the hillock and an ectopic spike initiation zone are simultaneously active, orthodromic action potentials generated at the hillock may encounter antidromic ectopic action potentials generated at the spike initiation zone, as they travel toward each other on the axon. Hodgkin and Huxley [1] showed that the voltage-gated sodium channels that depolarize the axon membrane are inactivated for a few milliseconds after the action potential. Thus, a refractory period follows each action potential during which neurons are inexcitable and therefore unable of generating another action potential. Consequently, colliding action potentials should annihilate as they reach each other’s refractory periods.

Tasaki’s pioneer experimental work performed on motor nerve fibers innervating the sartorius muscle of the toad [8], demonstrated early on that colliding action potentials annihilate each other, confirming numerical predictions of the

Hodgkin-Huxley model [1]. This phenomenon has since been extensively mentioned in the literature and observed in various types of biological axons in both vertebrates and invertebrates, including heart tissue [9], rat brain aminergic axons [10], cat locomotion sensory afferents [11], crab motor sensory neurons [12], rat nigral dopaminergic neurons [13], and reflection with annihilation [14, 15]. A different approach using soliton propagation in biological excitable media has proposed electromechanical waves as a means of signal propagation and that oppositely traveling impulses cross. In particular, a recent study using the electromechanical theory for nerve-pulse propagation, in conjunction with experimental measurements [16], has proposed that action potentials may not annihilate upon collision, but rather cross and continue to travel along the axon.

Whether action potentials traveling in opposite directions annihilate or cross is of relevance for a number of neuronal functions, as action potential annihilation can affect neuronal information encoding and transmission [5]. Additionally, collision tests for identifying orthodromic or antidromic action potentials have been widely used (see [17] for a review), with application in collision blocking [18, 19] and in the treatment of spinal cord injury along with chronic pain of peripheral origin [20].

Despite the ubiquitous presence of the action potential collision phenomenon in the literature, little has been done on the specific investigation of the topic. Here we present numerical simulations and experimental results aimed at reducing this gap and helping to elucidate the subject of colliding action potentials. We introduce an axonal multicompartmental model with the compartments represented by Hodgkin-Huxley equations [1], reciprocally connected to each other by electrical couplings [21]. The numerical simulations are capable of mimicking low frequency ectopic spiking with orthodromic and antidromic action potential propagation. They predict that colliding action potentials traveling in opposite directions annihilate and may not cross. We further discuss this matter

* wstein@ilstu.edu

in the context of axonal excitability and supernormality after action potential initiation for neurons of type I and type II. We also present results of experimental work performed on the earthworm ventral cord and the crustacean stomatogastric nervous system. Both the numerical simulations and the experimental outputs clearly and unambiguously indicate that annihilation is inevitable.

II. THE HODGKIN-HUXLEY MODEL REVISITED

The mathematical model developed by Alan Hodgkin and Andrew Huxley for the propagation of electric signals along a nerve axon is remarkable [1]. The equations are based on experimental measurements on the giant axon of the squid performed at a time when the technique for measuring membrane voltage dependent permeability was still in the works. The model has been extended and applied to numerous studies [22–27], has stimulated an enormous amount of research, and has also been extremely influential in advancing the field of neuronal science [28, 29]. The equations describe the neuron’s membrane as a capacitor in parallel with variable resistors (ionic channels more conveniently modeled as conductances) and Nernst potentials represented by batteries. There are differential equations for (i) the voltage difference $V(t)$ between the potentials inside and outside of the cell, (ii) the activation variable $n(t)$ for the K^+ , and the (iii) activation and (iv) inactivation variables for Na^+ , respectively $m(t)$ and $h(t)$. These equations are

$$C\dot{V} = I_{stim} - I_K - I_{Na} - I_L \quad (1)$$

$$I_{Na} = g_{Na}m^3h(V - E_{Na}) \quad (2)$$

$$I_K = g_Kn^4(V - E_K) \quad (3)$$

$$I_L = g_L(V - E_L) \quad (4)$$

$$\dot{n} = \frac{(n_\infty(V) - n)}{\tau_n(V)} \quad (5)$$

$$\dot{m} = \frac{(m_\infty(V) - m)}{\tau_m(V)} \quad (6)$$

$$\dot{h} = \frac{(h_\infty(V) - h)}{\tau_h(V)} \quad (7)$$

where the capacitance C is considered constant, the currents I_K and I_{Na} are identified by the corresponding subscripts, I_{stim} corresponds to the applied stimulus, I_L is an ohmic leak current term mostly for Cl^- ions [30]. The functions n_∞ , m_∞ and h_∞ are voltage-dependent time independent rate constants and describe the transition rates between open and closed states of the channels. And τ_n , τ_m and τ_h are voltage-dependent time constants (more detailed about these equations including parameter values are shown in Appendix A).

A. Neurons of type I and type II

The sodium channels initiating the action potential have two independent gates with opposing voltage dependencies.

As they initiate the action potential they also inactivate as a function of voltage (h_∞), therefore causing the refractory period that follows the action potential. This ‘recovery’ cycle is characterized by an initial sharp decrease in membrane excitability followed by a slow recovery that, in some cases, can exceed the resting state excitability (supernormality). As experimentally first detailed by Hodgkin [31], three different types of axons can be distinguished when current is injected into them: (I) Axons with recovery cycle where supernormal phase is not present, and firing rate varying smoothly in the approximate range from 5 to 150 Hz, (II) Axons with noticeable supernormal phase, relatively insensitive to a range in the strength of the applied current, and firing rate varying from 75 to 150 Hz, and (III) Axons displaying repetitive action potentials only at applied currents much stronger than the rheobase (the threshold current) [32]. Here we assess the first two types of behaviors with regard to ectopic action potential initiation. Ectopic spiking occurs at low firing frequencies of a few Hz [12]. Thus, type II and III axons are inadequate to describe ectopically firing axons as their firing occurs at frequencies below the minimum frequencies of neurons type II and III. Rather, the axons displaying ectopic spiking must be type I, or hybrid with both type I and type II with at least one compartment of type I capable of firing at low frequencies.

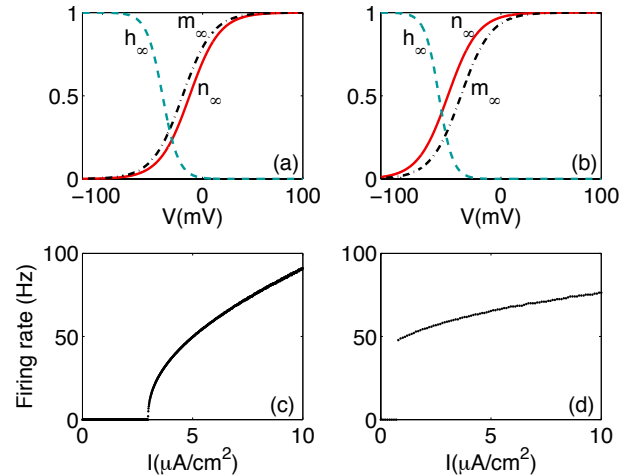


FIG. 1. (Color online) Steady-state functions for Na^+ gate activation (m_∞ , dot-dashed black line) and inactivation (h_∞ , dashed blue line) and K^+ gate inactivation (n_∞ , solid red line), as indicated, for neurons of type I (plot (a)) and of type II (plot (b)). Gain function ($f - I$ curves) showing the relation between input current and firing frequency for type I (plot (c)) and type II (plot (d)) neurons.

Type I and type II neurons here were generated by adjusting the corresponding steady-state functions for Na^+ gate activation (m_∞) and inactivation (h_∞), and K^+ gate activation (n_∞), as illustrated in Fig. 1 (a) and (b). Notice m_∞ , h_∞ and n_∞ shifted to more depolarized voltages in type I compared to type II. Figure 1(c) and (d) depicts the evolution of the firing rates as a function of a stimulus current injected into neurons of type I and type II, respectively. The minimum impulse for sufficient activation of the sodium channels to elicit

action potentials in type I and type II neurons are, respectively, $3 \mu\text{A}/\text{m}^2$ and $0.8 \mu\text{A}/\text{m}^2$, with respective frequencies of 1.9 Hz and 47.8 Hz. Interestingly, however, the type I axon not only was able to fire at lower firing frequencies than the type II axon, it also reached higher maximum firing frequencies. Thus, the dynamic range of the type II axon was significantly lower than that of the type I axon. The corresponding gate function and parameter values for both types are given in Appendix A.

Besides the steady state functions for gate activation, ion channel maximum conductance levels determine the firing behavior of a neuron [33]. To obtain a more comprehensive view of the firing rates associated with neurons of type I and type II we thus altered g_K and g_{Na} over a broad range. Figure 2 shows two color maps, depicting how the firing rates for the two types of neurons evolve with varying values of g_K and g_{Na} , all other parameters fixed at values as indicated in Appendix A.

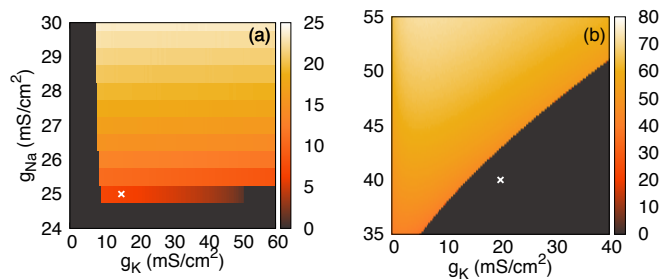


FIG. 2. (Color online) Parameter space color maps for (a) type I neuron with constant $I_{stim} = 3 \mu\text{A}/\text{cm}^2$, and for (b) type II neuron with no stimulus. The color bars on the right indicate the spiking frequency in Hz obtained for varying maximum sodium and potassium conductance levels.

The overall feature of increasing g_{Na} and decreasing g_K for faster firing is readily observed in Fig. 2(b) for type II neuron, whereas in the case of type I neuron shown in Fig. 2(a), decreasing the values of g_K did not increase the neuron's firing rate, except at the lowest values of the sodium conductance that still resulted in action potential initiation ($g_{Na} \simeq 25 \text{ mS}/\text{cm}^2$). The \times marks in Figs. 2 (a) and (b) indicate the maximum conductance values of the potassium and sodium used throughout this work for neurons type I and II, respectively.

B. Refractory period and consequences for axonal excitability

Pioneer voltage clamp experiments realized by Hodgkin and Huxley [1] indicated that depolarization in membrane potential causes a transient increase in the sodium conductance as well as in the, albeit slower, potassium conductance. Approximately at the time when the potassium conductance increases (at the peak voltage), the sodium conductance decreases dramatically due to the closing of the inactivation gate (compare Fig. 1(a), h_∞). As the membrane potential hyperpolarizes, the Na^+ channel activation gate quickly closes and

the inactivation gate slowly re-opens (de-inactivation), while the K^+ channel slowly closes. Hodgkin and Huxley's empirical approach for the mathematical description of the voltage-dependence of the membrane currents thus points to an *absolute* refractory period, approximately over the duration of the action potential, when Na^+ channels are inactivated. It renders the cell's membrane incapable of generating another action potential, even under the effect of a very strong stimulus. The *absolute* refractory period is followed by a *relative* refractory period during which the application of a stimulus stronger than the threshold current can generate an action potential. This happens as the Na^+ channels de-inactivate and the K^+ channels are still open.

In Fig. 3(a) and (b) we show, starting in time at the peak of an action potential, the minimum current needed to generate another action potential for neurons type I and type II, respectively. With the type I axon parameter combination, the absolute refractory period is longer than in the type II axon, i.e., the axon membrane remains inexcitable for a longer duration. Membrane excitability in the relative refractory period recovered following an exponential curve towards control values. The type II axon membrane excitability also shows an exponential recovery, however with a faster time constant and, in contrast to type I, excitability becomes supernormal before it returned to control values. This is demonstrated by a drop below threshold current in Fig. 3(b) and indicates that the membrane can be more excitable after an action potential than at rest. This supernormality has been described experimentally as well and is often discussed in terms of affecting action potential propagation speed [34–37]. Supernormality can increase action potential propagation speed because higher excitability allows action potentials to be elicited earlier (and thus faster) if they occur at times of supernormality. The fact that supernormality allows action potentials to be generated more easily in the wake of traveling action potentials may be interesting, in the light of collision of orthodromic and antidromic action potentials. It is typically thought that the refractory period prevents action potentials from propagating back to where they originated from and blocks a crossing of action potentials when they travel in opposite directions. Potentially, however, higher excitability in the wake of an action potential may allow oncoming action potentials to 'jump' across the refractory sections of the membrane and to continue to be propagated (without annihilation). To test whether the Hodgkin-Huxley model allows for this possibility we next created a multicompartment model of an axon.

III. AXONAL MODEL

Our axonal model consists of a linear chain of compartments with each compartment represented by Hodgkin-Huxley type equations [1], reciprocally coupled to each other by electric connections. The corresponding equations are

$$C\dot{V}_i = I_{stim} - g_K n_i^4 (V_i - E_K) - g_{Na} m_i^3 h_i (V_i - E_{Na}) - g_L (V_i - E_L) - g_{el} (V_i - V_{i-1}) - g_{el} (V_i - V_{i+1}) \quad (8)$$

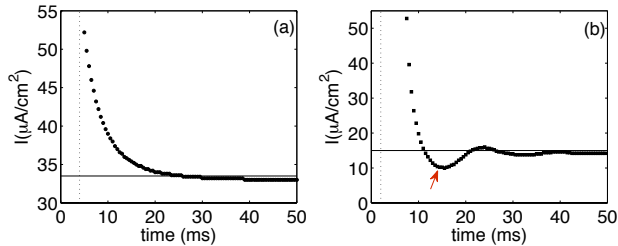


FIG. 3. Refractory period in the Hodgkin-Huxley model. The minimal current amplitude needed to evoke a second spike in (a) type I neuron and (b) type II neuron, plotted against the time after the first spike occurred. The rheobase amplitude to elicit the first action potential in type I is $34 \mu\text{A}/\text{cm}^2$ and $15 \mu\text{A}/\text{cm}^2$ in type II (indicated by the horizontal lines). The arrow indicates the region of supernormal excitability of type II neuron followed by a short subnormal period. The vertical dashed lines indicate the border between absolute and relative refractory period.

$$\dot{n}_i = \frac{(n_\infty(V_i) - n_i)}{\tau_n(V_i)} \quad (9)$$

$$\dot{m}_i = \frac{(m_\infty(V_i) - m_i)}{\tau_m(V_i)} \quad (10)$$

$$\dot{h}_i = \frac{(h_\infty(V_i) - h_i)}{\tau_h(V_i)} \quad (11)$$

where the subscript i corresponds to the compartment number and the terms $g_{el}(V_i - V_{i-1})$ and $g_{el}(V_i - V_{i+1})$ account for the reciprocal coupling between neighboring compartments with coupling strength g_{el} .

A. Action Potential Propagation

As passive membrane currents have an important functional role in electrical signaling in nerve cells including action potential propagation, it becomes relevant to have a quantitative understanding of how passive current flows evolve as the action potential travels along the axon. Since our type I and type II neurons have distinct parameter settings for g_{Na} and g_K , their excitability and response properties to excitatory current are quite different (see Fig. 1). Current flow along the axon is determined by the coupling parameters between compartments, therefore these parameters had to be adjusted for each type to allow action potential propagation along the axon trunk. For type I axon a coupling of $g_{el} = 0.7 \text{ mS}/\text{cm}^2$ was necessary to allow action potential propagation, while a coupling of $g_{el} = 0.25 \text{ mS}/\text{cm}^2$ was sufficient for type II.

In Fig. 4 we show the evolution of a sub threshold current, injected in the middle compartment of our model, undergoing dissipation in both directions due to leakage across the membrane. The decay of the membrane current flow in terms of distance can be described by $V_x = V_0 e^{-x/\lambda}$, where V_x is the voltage across the membrane at position x (here measured in units of *compartment*) on the axon, V_0 is the initial voltage response in the middle compartment (where the current is applied), and λ is the length constant of the axon. This length

constant corresponds to the distance for which the initial voltage V_0 decays to $1/e$, or 37% of its value.

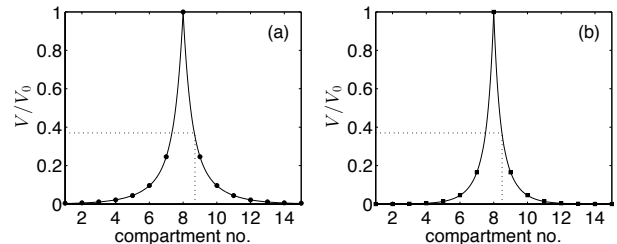


FIG. 4. Decay of the passive membrane potential as a function of the length of the axon trunk for (a) type I and for (b) type II axons. A sub-threshold stimulus applied in the middle of the axon (compartment no. 8) produced voltage responses V_x that decay exponentially with distance. The vertical dotted lines mark the length constants λ corresponding to $1/e$, or 37% of decay of the initial value of the voltage V_0 . In type II the decay is steeper than in type I.

For type I axon we obtained a value of $\lambda \simeq 0.5 \text{ compartment}$ (Fig. 4(a)) with a coupling constant of $0.7 \text{ mS}/\text{cm}^2$. In type II, with coupling $g_{el} = 0.38 \text{ mS}/\text{cm}^2$ we obtained $\lambda \simeq 0.7 \text{ compartment}$ (Fig. 4(b)). Using the same coupling in both axon types yielded very similar length constants.

To test whether the difference in membrane excitability between type I and II axons affects action potential propagation velocity we elicited action potentials in compartment 1 and tracked their propagation through the other compartments. The results are displayed in Fig. 5, where the same coupling $g_{el} = 0.7 \text{ mS}/\text{cm}^2$ was applied to axon type I in plot (a) and to axon type II in plot (b). Both axons exhibit the same $\lambda \simeq 0.7 \text{ compartment}$, but different action potential propagation speeds. We found that the action potential propagated more slowly, at $0.74 \text{ compartment}/\text{ms}$ for the type I neuron than it did for the type II which propagated at a speed of $1.18 \text{ compartment}/\text{ms}$. A weaker coupling, of $g_{el} = 0.38 \text{ mS}/\text{cm}^2$, was not enough for the action potential to propagate beyond the first compartment for the type I neuron in plot (c), and slowed down the type II neuron in plot (d) to a speed of $0.74 \text{ compartment}/\text{ms}$. This was the same propagation speed as the type I neuron in plot (a) achieved with a stronger coupling. Consequently, axons of type I and II can have similar action potential propagation speeds despite vastly different couplings between compartments, i.e., the combination of coupling and properties of sodium and potassium conductances determine propagation speed.

B. Action Potential Collision

Given the possibility of two action potentials traveling in opposite directions on the same axon trunk, we want to investigate whether they cross each other or collide and mutually annihilate. We used an axon model with nine compartments in three different configurations. First we applied a stimulus to compartment 1 and tracked the resulting action potential as it traveled through all compartments, as shown in Fig. 6(a),

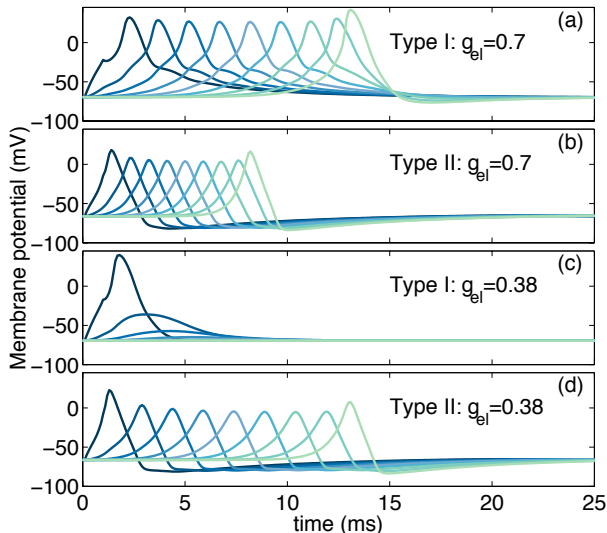


FIG. 5. (Color online) Action potential propagation along the axonal multicompartment model, with an action potential elicited in the first compartment to the left, (dark blue (black) line), propagating to the right all the way to the last (light blue (gray) line). Each shade corresponds to a different compartment, for a total of nine. All compartments within the same axonal type (I or II) are identical, identically connected to each other via reciprocal electric coupling and g_{el} values as shown. The axons for plots (a) and (b) are of types I and II, respectively, coupled with $g_{el} = 0.7$ mS/cm², displaying speeds of propagation of 0.74 compartment/ms in type I and 1.18 compartment/ms in type II. Plots (c) and (d) are also for neurons type I and II, respectively, but now coupled with $g_{el} = 0.38$ mS/cm², insufficient for the propagation of the action potentials of the type I axon in (c), and slowing down the propagation of the type II neuron in (d) to 0.74 compartment/ms. Note that the larger action potential amplitudes in compartments 1 and 9 were due to decreased leakage in these compartments resulting from the lack of further neighboring compartments.

(b) and (c). The different shades in the colors from dark to light serve to distinguish the actions potentials in the different compartments, starting at compartment 1 and ending at compartment 9. Second, as illustrated in Fig. 6(f), (e) and (d), the stimulus was applied to compartment 9, eliciting an action potential which then traveled along the axon all the way back to compartment 1. The colors here are associated with the different compartments in the same fashion as in the previous case, except that here the order in the color shade is from light to dark. Third, we simultaneously stimulated both compartments 1 (dark blue (black), plot (g)) and 9 (light green (gray), plot (l)), which generated action potentials traveling in opposite directions and meeting half-way through, in compartment 5 (plot (h)). Figure 6(g) is the equivalent of Fig. 6(a), and Fig. 6(i) is the equivalent of Fig. 6(f), both cases depicting action potentials traveling unopposed along the axon over three compartments. The action potentials of the 4th compartment (coming from the left, Fig. 6(b)) and of the 6th compartment (coming from the right, Fig. 6(e)) are equivalent, except for the fact that they are coming from opposite directions. However, the action potential of the 5th compartment shown in Fig. 6(h) was the last in both sequences, from the left and

from the right. After the action potentials met in compartment 5, the action potentials did not continue to either side.

Thus, despite the fact that type II neurons show supernormality, there was no follow-up action potential in either direction, i.e., action potentials did not cross after the collision. Rather, there was annihilation due to the refractory periods in the wake of the two colliding action potentials. Our model results thus indicate that the Hodgkin-Huxley axon model does not allow crossing of action potentials, independently of whether the axon is of type I or II. A previous study pointed out that in biological systems action potentials traveling in opposite directions may be able to cross without annihilation [16], suggesting that the Hodgkin-Huxley model may not be adequate for all types of axons. To further investigate the concept of action potential crossing in biological systems we carried out experiments in two well-studied nervous systems: the ventral nerve cord of the earthworm (*Eisenia hortensis*) and the stomatogastric nervous system of the crab (*Cancer borealis*). Both systems have been studied extensively [38–43] and used for measuring action potential propagation ([31, 44, 45].

IV. EXPERIMENTAL SETUP

The ventral nerve cord of the earthworm (*Eisenia hortensis*) and the axon of the lateral pyloric (LP) motor neuron of the stomatogastric nervous system of the crab (*Cancer borealis*) were used to study the dynamics of action potential propagation along the axon. Details about the materials and methods can be found in Appendix B.

A. Stimulation Protocol

Action potentials were elicited with pulses of 0.5 ms at different stimulation voltages. Threshold voltage was determined by gradually increasing the voltage until an action potential was generated. This threshold changes between stimulation sites and preparations due to differences in the size of the wells used and the axon diameter. Threshold was adjusted separately for each individual stimulation site. In this study we considered, for the Earthworm Ventral Nerve cord (EVN), two different experimental configurations, each with four wells placed along the nerve.

In configuration EVN1 the four wells sequence, from anterior to posterior, corresponds to recording, recording, stimulation and stimulation sites in this order, as depicted in Fig. 7(b), with the implementation of the following protocols consisting of three different procedures: (i) An action potential was elicited by stimulation at the most posterior stimulation site; (ii) An action potential was elicited by stimulating the middle posterior stimulation site; (iii) Two action potentials were elicited by stimulating both stimulation sites simultaneously. In configuration EVN2 the four wells as described in configuration EVN1 were used, from anterior to posterior, but now in a different order: recording, stimulation, recording and stimulation, as shown in Fig. 7(c), with the following protocols

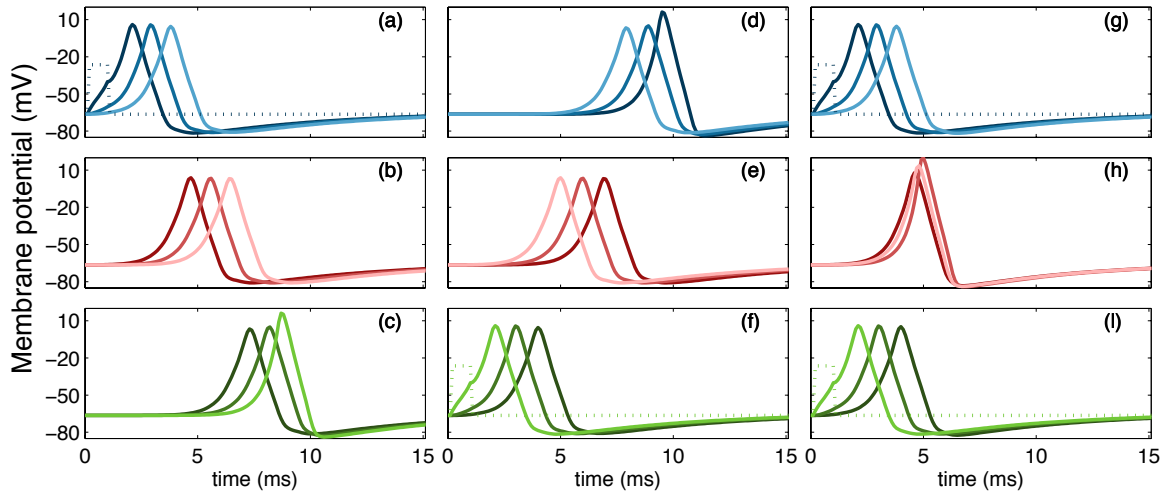


FIG. 6. (Color online) Response of a 9-compartment axon model to external stimulus in three different settings. Upper panels with colors ranging from dark blue (black) to light blue (gray) represent compartments 1 to 3, middle panels with colors ranging from dark red (black) to light red (gray) represent compartments 4 to 6, and bottom panels with colors ranging from dark green (black) to light green (gray) represent compartments 7 to 9. First, in plots (a), (b) and (c), an action potential elicited in compartment 1 travels unopposed to the right. Each action potential, with colors ranging from dark blue (black) to light blue (gray) in (a), from dark red (black) to light red (gray) in (b), and from dark green (black) to light green (gray) in (c), corresponds to the traveling action potential as it sequentially traverses each compartment. Second, in plots (f), (e) and (d), an action potential elicited in compartment 9 travels unopposed to the left. Third, in plots (g), (h) and (i), compartments 1 and 9 are stimulated simultaneously, generating action potentials that start at the two ends of the axon and travel toward each other, eventually meeting at the center, in compartment 5, unable to pass through to continue on other half.

consisting of three different procedures: i) An action potential was elicited by stimulation of the most posterior stimulation site; ii) An action potential was elicited by stimulating the middle anterior stimulation site; iii) Two action potentials were elicited by stimulating both stimulation sites simultaneously.

In both protocols described above, the two recording sites were outside of the stimulated area and hence allowed determining threshold voltage and success of the stimulation. They also allowed unambiguous identification of the stimulated axons by both action potential shape on two independent recordings and propagation velocity (determined by the action potential travel time between the two recording sites). This arrangement, with two recording sites, is particularly important because action potential annihilation can be shown directly while experiments using just one recording site rely solely on changes in the shape of the action potential [16]. In addition, the EVN contains multiple large diameter axons that may be activated by the applied extracellular stimulation. It is thus imperative to clearly identify which axon(s) have been stimulated.

For the crab LP motor neuron, the experimental configuration consisted of three wells with one stimulation located at the anterior dorsal ventricular nerve, *dvn*, another stimulation located more posterior at the lateral ventricular nerve *lvn*, followed by the most posterior recording located at the *lvn* (Fig.8). The stomatogastric nervous system is a well studied system with all axons contained within the *dvn* and *lvn* already identified [41, 42]. This offers several advantages over the EVN (and other nerve cords) preparation. In particular, the well-known spontaneous activity of the motor neurons al-

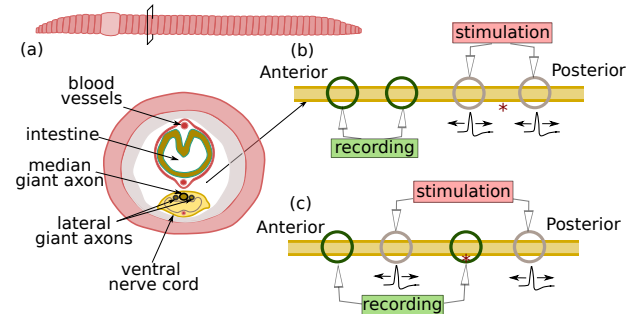


FIG. 7. (Color online) Schematic of (a) the ventral nerve cord of the earthworm, (b) EVN1 stimulation setup: two anterior recording sites and two posterior stimulations sites, (c) EVN2 stimulation setup: two recordings, one at anterior and another at middle posterior, and two stimulations sites, one at posterior and another at middle anterior. The asterisk (*) indicates where collisions may occur.

lows the unambiguous detection of action potential identity by shape, amplitude and velocity along the nerve. Before each experiment we thus used all three wells for recording the spontaneous activity and determining LP action potential shape, amplitude and delay between recordings. This then allowed us to calculate travel times from individual stimulation sites to the posterior recordings site in the collision experiment. Stimulation threshold was then chosen to specifically elicit LP action potentials.

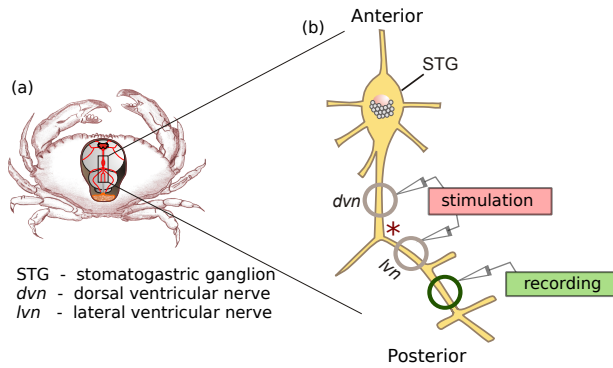


FIG. 8. (color online) The stomatogastric nervous system (STNS) of the crab, (*Cancer borealis*). (a) Dorsal view of the crab with parts of its dorsal carapace removed. (b) Representation of part of the isolated STNS. We consider the axon of the lateral pyloric (LP) motor neuron. Stimulation setup with two stimulation sites, one at *dvn* and another at *lvn*. Action potentials were recorded at the posterior *lvn*.

V. EXPERIMENTAL RESULTS

A. Earthworm

The earthworm ventral nerve (EVN) contains several large diameter axon fibers that span the entire nerve cord from posterior to anterior [38, 46]. The largest axons are those of the two lateral giant fibers and the median giant fiber. Typically, the medial fiber has the largest diameter and is thus recruited at lowest stimulation thresholds, while the two lateral fibers are only recruited at higher stimulation amplitudes. However, to test action potential collision, stimulation of the *same* axon at two different locations is required. To ensure unambiguous identification of the stimulated axons, we used an improved electrode placement in comparison to previous experiments: Two electrodes were used for recording the traveling action potentials, allowing to separate action potentials by propagation velocity (as measured by the time delay and spatial distance between electrodes) and by action potential shape at the two recording sites. In all experiments, we first activated (*i*) the stimulation site farthest from the recording sites, then (*ii*) the more proximal stimulation site, and finally (*iii*) both sites simultaneously (more details shown above in Section IV A). The first two protocols, (*i*) and (*ii*), reveal the action potential velocity and time of arrival at the recordings sites, and the final protocol (*iii*) causes the action potential between stimulation sites travel in opposite directions (anti- and orthodromically).

For configuration EVN1, the recording sites were anterior to the stimulations sites. When we stimulated the most posterior stimulation site in protocol (*i*), the action potential arrived first at the middle anterior recording site (closer to the stimulation site, Fig. 9(b)), and then at the anterior recording (most distal to the stimulation site, Fig. 9(a)). Similar results (Fig. 9(c)-(d)) were obtained when we stimulated the more anterior stimulation site with protocol (*ii*), except that since this stimulation site was closer to the recording sites the times for detection of the action potential were shorter than in the previous experiment (*i*). When both stimulation sites were ac-

tivated simultaneously we only observed the action potential elicited by stimulus site (*ii*) in both recordings (Fig. 9(e)-(f)). This suggested that the action potential elicited by the middle posterior stimulus, traveling to the posterior, collided with the action potential elicited at the posterior site and traveling to the anterior, resulting in mutual annihilation. These results are in agreement with the results obtained with our compartmental axon model. We obtained similar results in all preparations tested ($N=4$), indicating that all action potential collisions resulted in annihilation and that action potentials traveling in opposite direction never crossed.

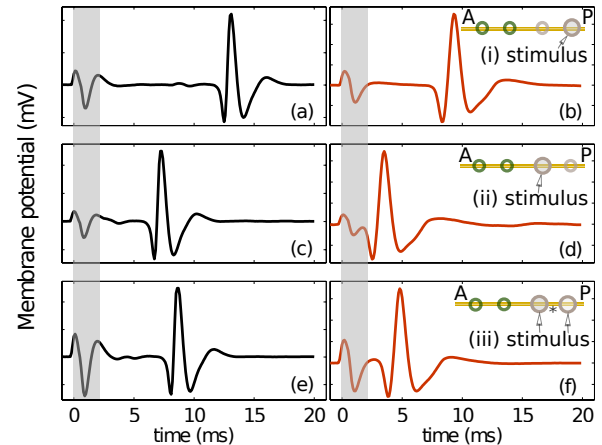


FIG. 9. (Color online) Earthworm experimental results for configuration EVN1 anterior to posterior: recording, recording, stimulation, stimulation. Plots (a), (c) and (e) are for action potential observed at anterior recording site, and plots (b), (d) and (f) are for action potential observed at middle anterior recording site. Action potentials were elicited with protocol (*i*): stimulus at the most posterior site; protocol (*ii*): stimulus at the middle posterior site; protocol (*iii*): stimulus at both sites simultaneously. The shaded region indicates the stimulus artifact.

To further examine action potential collision in the axon and whether a recording placed in-between stimulation sites can detect annihilation, we moved one of the recording sites to in-between the stimulation sites configuration EVN2, see Fig. 7(c). In this case, the (anterior) recording remaining outside the stimulation sites was used as a measure for annihilation (as in the experiments above) and the recording in-between sites was assessed for changes during this event. When we stimulated the most posterior site, the action potential arrived first at the recording site in-between stimulation sites (as it was closer to the stimulated site (*i*), (Fig. 10(b)) and then at the anterior recording site (Fig. 10(a)). Note that the differences in the shape of action potentials in Fig. 9 and Fig. 10 are due to different preparations and different well sizes.

When the more anterior stimulation site was activated, the action potential arrived again first at the recording site in-between stimulation sites (Fig. 10(c)) and with a delay at the anterior recording site (Fig. 10(d)). The delay was shorter than in protocol (*i*) since this stimulation site was closer to the anterior recording site. The delay to the recording site in-between

stimulation sites remained unchanged, as this recording site is located approximately in the middle of the stimulation sites and action potentials travel at similar velocities. Note that in this case, action potentials elicited at the anterior stimulation site, protocol (i), travel in opposite direction as those elicited by the posterior stimulation site, protocol (ii). When both stimulation sites were activated simultaneously (iii), the only action potential detected at the recording sites was the action potential elicited at the middle posterior stimulation site and traveling to the anterior, as shown in Figs. 10(e) and 10(f). Under this condition two action potentials were generated (one in each stimulation site), each traveling in both directions (anti- and orthodromic). As a result, the action potential elicited by the middle posterior stimulus, traveling to the posterior, collided with the action potential elicited at posterior, traveling to the anterior, leading to mutual annihilation.

We obtained similar results in all preparations tested ($N=4$): Action potentials propagating in opposite directions always collided and annihilated, indicating that the refractory period prevented action potential crossing. These experimental results in combination with the axon multicompartment model results further support the conclusion from the Hodgkin-Huxley model [1].

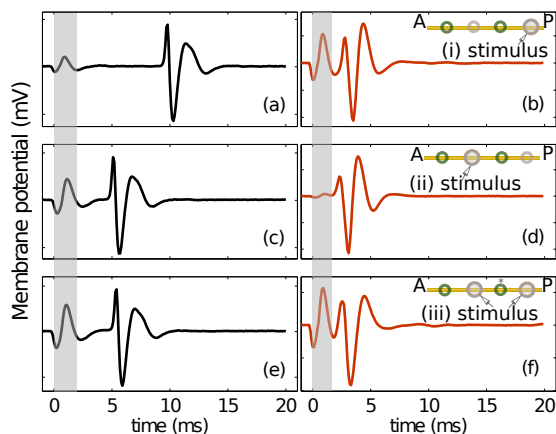


FIG. 10. (Color online) Earthworm experimental results with a recording site in-between stimulation sites. Configuration EVN2 anterior to posterior: recording, stimulation, recording, stimulation. (a),(c) and (e) action potential observed at anterior recording site, (b),(d) and (f) action potential observed at middle posterior recording site. Action potentials were elicited by protocol (i): stimulus at the most posterior stimulation site; protocol (ii): stimulus only at the middle anterior stimulation site; protocol (iii): stimulus at both stimulation sites simultaneously. The shaded region indicates the stimulus artifact.

B. Stomatogastric Nervous System

While action potential propagation in earthworm medial giant fibers has been studied for many decades, this system is not a good representation of a typical axon. The reason for this is that the fiber is actually not a single axon, but rather

results from the (electrical) coupling of individual axons during development. The axons of individual axons (one in each segment of the worm) are strongly coupled electrically across segment borders, allowing action potential propagation across segmental borders. At the same time, axons typically originate from one neuron, not many. Whether this difference affects action potential propagation and collision is unclear.

To further scrutinize action potential collision we thus used an identified axon in the stomatogastric nervous system. We stimulated the axon of the lateral pyloric neuron LP at two sites of the (*lvn*) and recorded the LP action potential at a site posterior to both stimulation sites. Figure 11(a) shows an action potential observed about 24 ms after the application of the stimulus at the anterior *dvn* site. Similarly, when an action potential was elicited by stimulating the *lvn* site, which was closer to the recording site, that action potential was detected earlier (about 10 ms), as shown in Fig. 11(b). When both stimulation sites were activated simultaneously, the only action potential detected at the recording site was the action potential elicited at the closer stimulation site, i.e., *lvn* (see Fig. 11(c)). Since action potentials can travel anti- and orthodromically, the action potential elicited at the anterior *dvn* site and propagating antidromically to the posterior collided with the action potential elicited at *lvn* propagating orthodromically. As a result these two action potentials annihilated each other.

In all our experiments ($N=4$) with the axon of the LP motor neuron we observed similar results. Action potentials propagating in opposite directions collided and did not cross. These observations reinforce the agreement between our axon model and the biological axon.

VI. DISCUSSION

Nerve fibers, or axons, are long projections of nerve cells often considered as mere cables through which electric impulses travel. Axons, however, do more than just transmitting electric impulses - they are actively involved in the encoding of neuronal information associated with the dynamics of propagation [5]. In fact, many axons can generate action potentials at ectopic locations, i.e., not at the axon hillock but somewhere else along the axon. These action potentials then travel both orthodromically and antidromically from their point of origin. Particularly well-studied examples are invertebrate axons that project between ganglia where action potentials can be initiated in each ganglion due to local synaptic input [4]. Ectopic action potentials can collide with action potentials generated at the hillock (for summary see [5]) and are thought to be annihilated upon collision. In the classical Hodgkin-Huxley model of action potential generation [1], the neuron's membrane undergoes a period of inexcitability after each action potential because of the inactivation of sodium channels (the refractory period). The membrane inexcitability trails behind the action potential as it propagates along the axon and prevents back-propagation. Therefore annihilation should be expected when action potentials traveling in opposite directions collide. Conversely, it has been suggested that some biological axons may show properties of crossing action potentials [16], and that

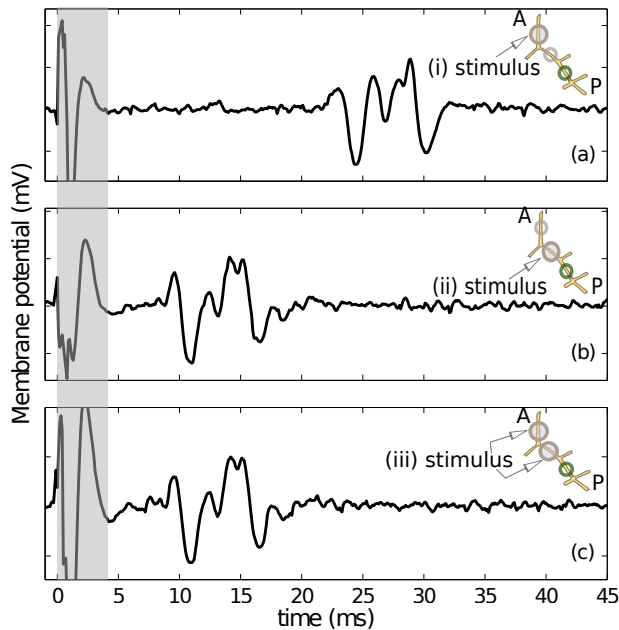


FIG. 11. (Color online) Crab experimental results for configuration anterior to posterior: stimulation site at *dvn*, another stimulation at *lvn* and a recording site at most posterior *lvn*. Action potential elicited by stimulating (a) only *dvn*, (b) only *lvn*, (c) both sites simultaneously. The shaded region indicates the stimulus artifact.

Hodgkin-Huxley type models may be inadequate for representing some axons. This view has recently been challenged in a study [47] demonstrating that in the particular case of small neurons, modeled with a reduced Hodgkin-Huxley system (Morris-Lecar equations [48, 49]), leading-order effects elicit soliton-like behaviors. In specific, by incorporating a variable Nernst potential into the conventional Morris-Lecar reaction-diffusion model, emergent complex spatiotemporal dynamics of axon excitability, including soliton-like behaviors, were demonstrated [47]. Thus, soliton-like regimes may be common in excitable membranes, and indeed there is experimental evidence in the form of action potential reflection at axon branch points [50]. Reflection [14] of colliding action potentials can also occur in numerical simulations with the Hodgkin-Huxley equations. Taken together, these studies inform us that there is no need of dispensing with the Hodgkin-Huxley underlying basis in order to observe such soliton-like behaviors.

Here we addressed the question of action potential collision using two different, but related, approaches. First, computationally, we performed numerical simulations with mathematical equations implemented on an axonal multicompartment model where each compartment is represented by the Hodgkin-Huxley equations. The compartments were connected to their neighbors via electrical coupling, in a linear chain format, where action potentials can travel in one direction or the other along the chain. The Hodgkin-Huxley equations we used possess features with demonstrated capability for mimicking the dynamical evolution of the voltage differ-

ence across the membrane of the neuron. Typically, axons are thought to be of type II [30], i.e., display rather high firing frequencies once the threshold is crossed (Fig. 1). However, in axons where ectopic firing occurs at low frequencies, axon properties must be reminiscent of type I to support the low firing frequencies. Our axon model could be readily modified to show either type I or II behavior by changing the sodium and potassium maximum conductance values, in connection with the corresponding activation and inactivation functions. Both types I and II displayed a refractory period of about the duration of an action potential, indicating that when propagating in opposite directions, action potentials should collide and annihilate each other. However, the type II axons showed supernormality during the recovery phase of the refractory period, i.e., the membrane exhibited higher excitability than at rest. This feature could, in principle, allow action potentials traveling in opposite directions to go through each other's refractory period without reciprocal annihilation. Our multicompartmental model demonstrated that this was not the case. To test this prediction, we carried out collision experiments with the medial giant axon in the ventral nerve cord of the earthworm and with an identified motor axon in the crustacean stomatogastric nervous system. While the first is part of a fast escape response circuit, axons in the stomatogastric nervous system are capable of firing low frequency ectopic action potentials [4, 12] and are thus type I neurons. In carefully designed and appropriately implemented experiments we unambiguously determined that stimulated and recorded action potentials were indeed traveling in opposite directions on the same axon (guaranteeing no independent activation of different axons in the nerve cord). Consequently, action potential crossing or annihilation was clearly identifiable, and yet we detected no crossing of action potentials at all, in any of our experiments, in agreement with our numerical simulations and previous studies [12].

Our finding of action potential collision annihilation, using a multicompartment axonal model based on the Hodgkin-Huxley equations, is in clear contrast with the crossing found in the soliton model of Ref. [16]. The latter result is as expected since conservation laws preclude annihilation in colliding waves. Particularly, in a one-dimensional model, solitons succeed in avoiding destruction [14]. Also, our experimental results differ sharply from those of Ref. [16] in that we were unable to reproduce action potential crossing. This is despite the fact that the same experimental system (earthworm ventral nerve cord) was used. While in the experiments of Ref. [16] action potential crossing was assessed with a single recording electrode at the collision site, we used two recording sites spatially distant from the collision site. First, this allowed the unambiguous identification of the stimulated and recorded axon, guaranteeing the selective and specific activation and recording of a single rather than multiple axons in the nerve cord. Second, the experimental design produces an unambiguous result since action potentials either arrive at the recording site (in the case of crossing) or do not arrive (in the case of annihilation). We were particularly curious about the medial giant fiber, as it is not a single axon, but rather consists of fused axons of multiple neurons. Consequently this fiber may show

inhomogeneous regions as it passes through the nerve cord allowing for changes in excitability and/or resistance [51]. These changes are consistent with the idea of soliton-like behavior such as action potential reflection or crossing [51, 52], especially given the supernormality regime following action potentials of fast axons. However, we did not observe soliton-like behavior. With respect to the slower (type I) axons, for which our model also predicted the absence of action potential crossing, we tested the slow LP motor neuron in the crustacean STNS. This axon is also the neurite of a single neuron and thus a more typical axon. Here also action potential annihilation always occurred, confirming our model prediction.

Our results do not exclude the possibility that biological action potentials may show soliton-like behavior during action potential collision under certain conditions. Tanking into account the absence of experimental evidence we find this unlikely, at least in standard conditions. However, there are numerous reports of complex membrane properties in the axon trunk, owing to the presence of a multitude of different ion channels [53, 54]. Axons, both myelinated and unmyelinated, can be endowed with ionotropic and metabotropic receptors for transmitters and neuromodulators [5, 55], as well as a plethora of voltage-gated ion channels other than the Hodgkin-Huxley Na- and K-channels [5]. Ionotropic and metabotropic actions on these ion channels can cause changes in conduction velocities and may induce spike failures or initi-

ate extra action potentials somewhere along the axon (ectopic spike initiation) [3, 5, 55–58]. Consequently, spike propagation dynamics and collision behavior may be significantly influenced by such changes in intrinsic properties, in particular if channel densities change. For example, supernormality may be affected by the presence of additional channels. While passive capacitive effects contribute to supernormal conduction, persistent sodium currents can also play an important role [59, 60]. Furthermore, an accumulation of extracellular potassium and the subsequent change in the potassium Nernst potential may be involved in changing axon properties [61–64], making the study of modified Hodgkin-Huxley models such as in Ref. [47] necessary for determining axon propagation dynamics. This is particularly true given the presence of various metabotropic receptors in the axonal membrane, rendering axon properties conditional to the neuromodulatory state at hand.

ACKNOWLEDGMENTS

This work was supported by DFG STE 937/9-1, NSF IOS 1354932 and a cross-disciplinary grant of Illinois State University. Our numerical simulations were performed using an updated version of a computer code written by Quinton Skilling.

-
- [1] A. L. Hodgkin and A. F. Huxley, *J. Physiol.* **117**, 500 (1952).
 [2] J. F. Toennies, *J. Neurophysiol.* **1**, 378 (1938).
 [3] F. G. Standaert, *J. Gen. Physiol.* **47**, 53 (1963).
 [4] P. Meyrand, J. M. Weimann, and E. Marder, *J. Neurosci.* **12**, 2803 (1992).
 [5] D. Bucher and J.-M. Goaillard, *Prog. Neurobiol.* **94**, 307 (2011).
 [6] C. Gnay, F. H. Sieling, L. Dharmar, W.-H. Lin, V. Wolfram, R. Marley, R. A. Baines, and A. A. Prinz, *PLoS Comput. Biol.* **11**, e1004189 (2015).
 [7] S. Keros and J. Hablitz, *Neuroscience* **131**, 833 (2005).
 [8] I. Tasaki, *Biochimica et biophysica acta* **3**, 494 (1949).
 [9] B. M. Steinhaus, K. W. Spitzer, and S. Isomura, *IEEE Trans. Biomed. Eng.*, 731 (1985).
 [10] G. Aston-Jones, M. Segal, and F. E. Bloom, *Brain Rev.* **195**, 215 (1980).
 [11] S. Rossignol, R. Dubuc, and J.-P. Gossard, *Physiol. Rev.* **86**, 89 (2006).
 [12] N. Daur, F. Nadim, and W. Stein, *Eur. J. Neurosci.* **30**, 808 (2009).
 [13] A. Grace and B. Bunney, *Neuroscience* **10**, 301 (1983).
 [14] O. Aslanidi and O. Mornev, *J. Exp. Theor. Phys. Lett.* **65**, 579 (1997).
 [15] S. A. Baccus, *Proc. Natl. Acad. Sci. USA* **95**, 8345 (1998).
 [16] A. Gonzalez-Perez, R. Budvytyte, L. D. Mosgaard, S. Nissen, and T. Heimburg, *Phys. Rev. X* **4**, 031047 (2014).
 [17] D. Pinault, *Brain Res. Rev.* **21**, 42 (1995).
 [18] C. Van Den Honert and J. T. Mortimer, *IEEE Trans. Biomed. Eng.* **5**, 373 (1981).
 [19] T. Crish, J. Sweeney, and J. Mortimer, “Antidromic pulse generating wave form for collision blocking,” (1986), US Patent 4,608,985.
 [20] X. Zhang, J. R. Roppolo, W. C. De Groat, and C. Tai, *IEEE Trans. Biomed. Eng.* **53**, 2445 (2006).
 [21] E. Rosa, Q. M. Skilling, and W. Stein, *Biosystems* **127**, 73 (2015).
 [22] J. Foss, A. Longtin, B. Mensour, and J. Milton, *Phys. Rev. Lett.* **76**, 708 (1996).
 [23] H. Sakaguchi, *Phys. Rev. E* **73**, 031907 (2006).
 [24] T. Pereira, M. S. Baptista, J. Kurths, and M. B. Reyes, *Int. J. Bifurcat. Chaos* **17**, 3545 (2007).
 [25] S. Postnova, E. Rosa Jr, and H. Braun, *Pharmacopsychiatry* **43**, S82 (2010).
 [26] G. P. Krishnan, M. Bazhenov, and A. Pikovsky, *Phys. Rev. E* **88**, 042902 (2013).
 [27] T. d. L. Prado, S. Lopes, C. Batista, J. Kurths, and R. Viana, *Phys. Rev. E* **90**, 032818 (2014).
 [28] S. G. Waxman, *J. Physiol.* **590**, 2601 (2012).
 [29] D. Noble, A. Garny, and P. J. Noble, *J. Physiol.* **590**, 2613 (2012).
 [30] E. M. Izhikevich, *Dynamical systems in neuroscience: The Geometry of Excitability and Bursting* (MIT press, 2007).
 [31] A. Hodgkin, *J. Physiol.* **107**, 165 (1948).
 [32] F. Skinner, *F1000Research* **2**, 19 (2013).
 [33] A. A. Prinz, C. P. Billimoria, and E. Marder, *J. Neurophysiol.* **90**, 3998 (2003).
 [34] R. S. Zucker, *J. Physiol.* **241**, 111 (1974).
 [35] S. Raymond, *J. Physiol.* **290**, 273 (1979).
 [36] N. Stockbridge and N. Yamoah, *J. Mathematic. Biol.* **28**, 487 (1990).
 [37] R. Miller and J. Rinzel, *Biophys. J.* **34**, 227 (1981).
 [38] H. B. Stough, *J. Comp. Neurol.* **40**, 409 (1926).

- [39] W. Rushton, Proc R Soc Lond. Series B-Biological Sciences **132**, 423 (1945).
- [40] M. P. Nusbaum and M. P. Beenhakker, Nature **417**, 343 (2002).
- [41] E. Marder and D. Bucher, Annu. Rev. Physiol. **69**, 291 (2007).
- [42] W. Stein, J. Comp. Physiol. A **195**, 989 (2009).
- [43] R. M. Harris-Warrick, Curr. Opin. Neurobiol. **21**, 685 (2011).
- [44] K. M. Shannon, G. J. Gage, A. Jankovic, W. J. Wilson, and T. C. Marzullo, Adv. Physiol. Ed. **38**, 62 (2014).
- [45] A. W. Ballo and D. Bucher, J. Neurosci. **29**, 5062 (2009).
- [46] W. N. Hess, J. Morphol. **40**, 235 (1925).
- [47] S. R. Meier, J. L. Lancaster, and J. M. Starobin, PloS one **10**, e0122401 (2015).
- [48] C. Morris and H. Lecar, Biophys. J. **35**, 193 (1981).
- [49] H. Lecar, G. Ehrenstein, and R. Latorre, Ann. NY Acad. Sci. **264**, 304 (1975).
- [50] S. A. Baccus, B. D. Burrell, C. L. Sahley, and K. J. Muller, J. Neurophysiol. **83**, 1693 (2000).
- [51] D. Debanne, Nature Rev. Neurosci. **5**, 304 (2004).
- [52] J. W. Moore and M. Westerfield, J. Physiol. **336**, 285 (1983).
- [53] B. P. Bean, Nature Rev. Neurosci. **8**, 451 (2007).
- [54] B. D. Clark, E. M. Goldberg, and B. Rudy, Neuroscientist **15**, 651 (2009).
- [55] H. A. Swadlow, J. D. Kocsis, and S. G. Waxman, Annu. Rev. Biophys. Bioeng. **9**, 143 (1980).
- [56] F. G. Standaert, J. Gen. Physiol. **47**, 987 (1964).
- [57] T. H. Bullock, Annu. Rev. Physiol. **13**, 261 (1951).
- [58] H. A. Swadlow and S. G. Waxman, Exp. Neurol. **53**, 128 (1976).
- [59] H. Bostock and J. Rothwell, J. Physiol. **498**, 277 (1997).
- [60] C. C. McIntyre, A. G. Richardson, and W. M. Grill, J. Neurophysiol. **87**, 995 (2002).
- [61] C. M. Bower, J. D. Kocsis, E. F. Targ, and S. G. Waxman, Ann. Neurol. **22**, 264 (1987).
- [62] R. Gilliatt and R. Willison, J. Neurol. Neurosurg. Psychiatry **26**, 136 (1963).
- [63] J. Kocsis, R. Malenka, and S. Waxman, J. Physiol. **334**, 225 (1983).
- [64] D. Burke, I. Mogyoros, R. Vagg, and M. C. Kiernan, Brain **121**, 1975 (1998).
- [65] R. Harris-Warrick, E. Marder, A. Selverston, and M. Moulins, *The stomatogastric nervous system: a model biological neural network* (MIT Press, Boston, 1992).
- [66] W. S. Hoar and H. Cleveland Pendleton, *A Laboratory Companion for General and Comparative Physiology* (Englewood Cliffs, N.J.: Prentice-Hall, 1975).
- [67] G. J. Gutierrez and R. G. Grashow, J. Vis. Exp. **25**, 1207 (2009).
- [68] W. Stein, C. R. Smarandache, M. Nickmann, and U. B. Hedrich, J. Exper Biol. **209**, 1285 (2006).

Appendix A: Type I and Type II parameters

Type I neuron gate functions and time function

$$n_{\infty} = 1/(1 + \exp((-13 - V)/15)) \quad (\text{A1})$$

$$\tau_n = 1.1 + 4.7 \exp(-((-79 - V)/50)^2) \quad (\text{A2})$$

$$m_{\infty} = 1/(1 + \exp((-20 - V)/15)) \quad (\text{A3})$$

$$\tau_m = 0.04 + 0.46 \exp(-((-38 - V)/30)^2) \quad (\text{A4})$$

$$h_{\infty} = 1/(1 + \exp((-40 - V)/ - 8)) \quad (\text{A5})$$

$$\tau_h = 1.2 + 7.4 \exp(-((-67 - V)/20)^2) \quad (\text{A6})$$

Parameters:

$$g_K = 15 \text{ mS/cm}^2, \quad E_K = -90 \text{ mV}$$

$$g_{Na} = 25 \text{ mS/cm}^2, \quad E_{Na} = 50 \text{ mV}$$

$$g_L = 0.3 \text{ mS/cm}^2, \quad E_L = -70 \text{ mV}$$

$$C = 1 \text{ } \mu\text{F/cm}^2$$

Type II neuron gate functions and time function

$$n_{\infty} = 1/(1 + \exp((-53 - V)/15)) \quad (\text{A7})$$

$$\tau_n = 1.1 + 4.7 \exp(-((-79 - V)/50)^2) \quad (\text{A8})$$

$$m_{\infty} = 1/(1 + \exp((-40 - V)/15)) \quad (\text{A9})$$

$$\tau_m = 0.04 + 0.46 \exp(-((-38 - V)/30)^2) \quad (\text{A10})$$

$$h_{\infty} = 1/(1 + \exp((-62 - V)/ - 7)) \quad (\text{A11})$$

$$\tau_h = 1.2 + 7.4 \exp(-((-67 - V)/20)^2) \quad (\text{A12})$$

Parameters:

$$g_K = 20 \text{ mS/cm}^2, \quad E_K = -90 \text{ mV}$$

$$g_{Na} = 40 \text{ mS/cm}^2, \quad E_{Na} = 50 \text{ mV}$$

$$g_L = 1.5 \text{ mS/cm}^2, \quad E_L = -70 \text{ mV}$$

$$C = 1 \text{ } \mu\text{F/cm}^2$$

Appendix B: Materials and Methods

1. Animals

Earthworms (*Eisenia hortensis*) were obtained from local bait shops and maintained in hydrated soil at 3-5°C. Earthworms were anesthetized by keeping them immersed in a 10% ethanol solution for approximately 5-10 minutes before dissection. Adult crabs (*Cancer borealis*) were obtained from The Fresh Lobster Company (Gloucester, MA, USA) or Ocean Resources Inc. (Sedgwick, ME, USA). Crabs were kept in tanks with artificial sea water (salt content, 1.025 g/cm³) at a temperature of 10-12°C and a 12-hour light-dark cycle. Before dissection, animals were anesthetized on ice for 20-40 minutes. Conventional stomatogastric nervous system dissections were performed [65].

2. Solutions

Physiological crab saline consisted of: NaCl, 440 mM; KCl, 11 mM; MgCl₂ · 6H₂O, 26 mM; CaCl₂, 13 mM; tris base, 10 mM; maleic acid, 5 mM (pH 7.4-7.6). Earthworm saline consisted of: NaCl, 103 mM; KCl, 1.6 mM; CaCl₂, 1.4 mM; NaHCO₃, 1.2 mM (pH 7.6-7.8) [66].

3. Preparation and electrophysiology

Earthworm: After being anesthetized, the earthworm was pinned down in a dissection pan with the ventral side faced

down. The dorsal side was opened along the entire length of the earthworm body. Once open, the gut was carefully removed in order to not damage the ventral nerve cord located underneath. We also removed the ventral blood vessel lying over the ventral nerve cord. Subsequently we cut the lateral nerves to release the ventral nerve cord. Then the nerve cord was pinned down on a silicone elastomer-lined (ELASTOSIL RT-601, Wacker, Munich, Germany) Petri dish. Experiments were carried out on the isolated ventral nerve cord (Fig. 7) using standard electrophysiology methods.

For extracellular action potentials recordings, we used petroleum jelly wells built around a section of the nerve cord to electrically isolate it from the bath. Subsequent measurements of field potential changes were made between two stainless steel wires (one inside and one outside of each well). The differential signal was recorded, filtered and amplified with an AC differential amplifier (A-M Systems Modell 1700, Carlsborg, WA, USA). Files were recorded, saved and analyzed us-

ing Spike 2 Software (version 7.13; CED, Cambridge, UK) and a Micro1401 mkII. To elicit action potentials we stimulated extracellularly a section of the nerve cord, isolated with petroleum jelly wells, with pulses of 0.5ms duration at a frequency of 1Hz. A Spike 2 script was used to set the stimulus frequency and voltage.

Crab: The dissection was carried out as described in Gutierrez and Grashow [67]. In short, the STNS was pinned down on a silicone elastomer-lined Petri dish and continuously superfused (7-12 ml/min) with chilled saline (10-13°C). Experiments were performed on the isolated nervous system (Fig. 8) as described previously [68].

Similar to the earthworm, extracellular recordings and stimulation were performed with petroleum jelly wells around sections of the nerve. We recorded the lateral ventricular nerve, the main motor containing most motor axons of this system [42]. Action potentials were elicited by extracellular stimulations at the anterior dorsal ventricular nerve (*dvn*) and *lvn*.